Dewan Riset & Pengabdian kepada Masyarakat

Growth and Reaction Mechanism of Solution-Processed Cu2ZnSnSe4 Thin Films for Realizing Efficient Photovoltaic ap...

Growth and Reaction Mechanism of Solution-Processed Cu2ZnSnSe4 Thin Films for Realizing Efficient Photovoltaic applications

Document Details

Submission ID
trn:oid:::3618:147678298

Submission Date
Aug 8, 2026, 2:26 PM GMT+7

Download Date
Aug 8, 2026, 2:36 PM GMT+7

File Name
Growth and Reaction Mechanism of Solution-Processed Cu2ZnSnSe4 Thin Films for Realizing Eff....docx

File Size
2.5 MB

31 Pages

7,784 Words

42,546 Characters

11% Overall Similarity

The combined total of all matches, including overlapping sources, for each database.

Filtered from the Report

- Bibliography
- Quoted Text

Exclusions

- 21 Excluded Matches

Match Groups

39 Not Cited or Quoted 10%
Matches with neither in-text citation nor quotation marks

4 Missing Quotations 1%
Matches that are still very similar to source material

0 Missing Citation 0%
Matches that have quotation marks, but no in-text citation

0 Cited and Quoted 0%
Matches with in-text citation present, but no quotation marks

Top Sources

6% Internet sources
8% Publications
5% Submitted works (Student Papers)

Integrity Flags

0 Integrity Flags for Review

Our system's algorithms look deeply at a document for any inconsistencies that would set it apart from a normal submission. If we notice something strange, we flag it for you to review.

A Flag is not necessarily an indicator of a problem. However, we'd recommend you focus your attention there for further review.

Match Groups

- **39** Not Cited or Quoted 10%
  Matches with neither in-text citation nor quotation marks
- **4** Missing Quotations 1%
  Matches that are still very similar to source material
- **0** Missing Citation 0%
  Matches that have quotation marks, but no in-text citation
- **0** Cited and Quoted 0%
  Matches with in-text citation present, but no quotation marks

Top Sources

6% Internet sources
8% Publications
5% Submitted works (Student Papers)

Top Sources

The sources with the highest number of matches within the submission. Overlapping sources will not be displayed.

1	Publication	Narjes Beigom Mortazavi Amiri, Andrei Postnikov. " Secondary phase Cu SnSe vs... <1%
2	Internet	iopscience.iop.org <1%
3	Publication	Md. Akhtaruzzaman, Mohammad Ismail Hossain, Mohammad Aminul Islam, Md. ... <1%
4	Publication	Samiya Mahjabin, Md. Mahfuzul Haque, Sobayel Khan, Vidhya Selvanathan et al. "... <1%
5	Publication	Mohammad Ismail Hossain, Md. Shahiduzzaman, Safayet Ahmed, Md. Rashedul H... <1%
6	Student papers	University Der Es Salaam on 2018-10-10 <1%
7	Student papers	The Hong Kong Polytechnic University on 2017-06-28 <1%
8	Internet	dspace-unipr.cineca.it <1%
9	Internet	pureadmin.unileoben.ac.at <1%
10	Internet	transparencia.guadalajara.gob.mx <1%

11	Publication	ying liu, Xiaowei Xu, Ke Liu, Huihong Liu. "Synthesis of Cu2ZnSnSe4 thin film solar... <1%
12	Student papers	Queen Mary and Westfield College on 2013-04-25 <1%
13	Publication	Stenny Benny, Akshay Vishwanathan Vidyanagar, S. Venkataprasad Bhat. "Progre... <1%
14	Publication	Xianzhong Lin, Jaison Kavalakkatt, Martha Ch. Lux-Steiner, Ahmed Ennaoui. " Air-... <1%
15	Publication	Y.E. Romanyuk, C.M. Fella, A.R. Uhl, M. Werner, A.N. Tiwari, T. Schnabel, E. Ahlswe... <1%
16	Internet	qspace.library.queensu.ca <1%
17	Publication	Qing Zhou, Junhui Hei, Jiahui Ma, Zihang Liu et al. "Controllable in situ sodium do... <1%
18	Publication	Xiatong Qin, Bin Xu, Jianjun Lin, Jiaqi Chen, Hanyu Tong, Ye Chen, Pingxiong Yang... <1%
19	Internet	eprints.lib.hokudai.ac.jp <1%
20	Internet	strathprints.strath.ac.uk <1%
21	Internet	theses.lib.polyu.edu.hk <1%
22	Internet	unsworks.unsw.edu.au <1%
23	Publication	Mohammad Ismail Hossain, Haris Ahmad Khan, Masayuki Kozawa, Wayesh Qaro... <1%
24	Student papers	University of Liverpool on 2017-05-03 <1%

25 Student papers
University of Melbourne on 2024-06-02 <1%

26 Publication
"Copper Zinc Tin Sulfide-Based Thin-Film Solar Cells", Wiley, 2014 <1%

27 Publication
Shreyash Hadke, Menglin Huang, Chao Chen, Ying Fan Tay, Shiyou Chen, Jiang Ta... <1%

28 Student papers
Yeungnam University on 2019-11-25 <1%

29 Internet
files.core.ac.uk <1%

30 Student papers
University of Durham on 2014-11-06 <1%

31 Internet
ebin.pub <1%

32 Internet
www.researchgate.net <1%

33 Publication
"Advanced Characterization Techniques for Thin Film Solar Cells", Wiley, 2016 <1%

34 Publication
A.M. Islam, S. Islam, K. Sobayel, E.I. Emon, F.A. Jhuma, M. Shahiduzzaman, Md. Ak... <1%

35 Student papers
Chang Gung University on 2018-08-30 <1%

36 Publication
Tan, Joel Ming Rui, Yih Hong Lee, Srikanth Pedireddy, Tom Baikie, Xing Yi Ling, an... <1%

37 Internet
scholar.uoc.ac.in <1%

Growth and Reaction Mechanism of Solution-Processed $Cu_2ZnSnSe_4$ Thin Films for Realizing Efficient Photovoltaic applications

Ersan Y. Muslih[1,8,], K. Sobayel [2,*], Mohammad Ismail Hossain[3], Mohammad Junaebur Rashid[4,5], Hend I. Alkhammash[6], Badrul Munir[7], Md. Shahiduzzaman[8,*], Jean Michel Nunzi[8], Md. Akhtaruzzaman[2], Kim Kyoo Ho[9], and Tetsuya Taima[8]*

[1]Mechanical Engineering Department, Faculty of Industrial Technology, Trisakti University, Jakarta 11440. Indonesia

[2]Solar Energy Research Institute, The National University of Malaysia, 43600 Bangi, Selangor, Malaysia

[3]Department of Materials Sciences and Engineering, City University of Hong Kong, Kowloon, Hong Kong

[4]Department of Electrical and Electronic Engineering, University of Dhaka, Dhaka 1000, Bangladesh

[5]Semiconductor Technology Research Center, University of Dhaka, Dhaka 1000, Bangladesh

[6]Department of Electrical Engineering, College of Engineering, Taif University, P.O.Box 11099, Taif 21944, Saudi Arabia

[7]Department of Metallurgy and Materials Engineering, Universitas Indonesia, Depok, Indonesia

[8]Graduate School of Natural Science and Technology, Kanazawa University, Kakuma, Kanazawa 920-1292, Japan

[9]School of Material Science and Engineering, Yeungnam University, 214-1 Daedong, Gyeongsan, Gyeongbuk 712-749, South Korea.

*Corresponding authors: ersan.ym@trisakti.ac.id; sobayel@ukm.edu.my; shahiduzzaman@se.kanazawa-u.ac.jp

Abstract

The study reports the high-quality Cu2ZnSnSe4 (CZTSe) thin-film deposition by a non-hydrazine, non-pyridine, and environment-friendly low-cost solution process technique, then following the selenization process. The CZT film precursor was prepared from metal salts (Cu^{2+}, Zn^{2+}, and Sn^{4+}) in monoethanolamine (MEA) and ethanol mixture solvent annealed at 200 °C for 15 minutes under ambient atmosphere. Next, selenium was added to the CZT film precursor by selenization under Ar (95%) + H_2 (5%) atmosphere at 550 °C for 120 minutes. A detailed explanation of the growth and reaction mechanism is provided. The characterization results confirmed that the deposited CZTSe film was formed with high-crystallinity without carbon residue and excellent optoelectronic properties, which is undeniably suitable as an absorber for the photovoltaic application. The study further investigated CZTSe solar cell's photovoltaic properties using prepared CZTSe thin-film as an active layer. The electrical effects of solar cells are examined by the SCAPS simulation, where the optics of the device is investigated by finite-difference time-domain (FDTD) simulations in three-dimension. The investigations allow us to estimate the power conversion efficiency of CZTSe solar cells up to 18.5%. Detailed discussion on the device design and numerical calculations are provided.

***Keywords**:* CZTSe, non-hydrazine, solution process, SCAPS, FDTD.

1. Introduction

The kesterite solar cells such as Cu_2ZnSnS_4 (CZTS), $Cu_2ZnSnSe_4$ (CZTSe), and $Cu_2ZnSn(S,Se)_4$ are considered to be promising absorber materials for next-generation solar cell technology due to their earth abundance and low-cost processing methods [1-3]. However, the present power conversion efficiency (PCE) of such solar cells is limited to only

11~12% [1-3]. The photovoltaic performance of solar cells substantially relies on the absorber films' quality and their deposition processes. Until now, the PCE of CZTS solar cells reached up to 11.01% by evaporation [1], where CZTSe and CZTSSe solar cells demonstrated PCEs of 10.54% and 12.6%, respectively, by hydrazine addition [2,3]. In the case of CZTSe solar cells, thin-film can also be prepared by thermal evaporation, sputtering, electrodeposition, and solution process technique [4-10]. Nevertheless, high PCE from CZTSe solar cells can be realized by the solution process method with hydrazine [3]. Hydrazine is a non-carbon organic compound that can act as a solvent for many organic or inorganic compounds [11]. Because of its unique property, hydrazine is a prominent solvent for synthesizing selenium-based kesterite film (e.g., CZTSe), making larger high grain, uniformity of layer properties, and low wastage of raw materials [11,12]. In contrast, deposition using a hydrazine solvent also has some disadvantages, such as flammable, corrosive, acutely toxic, carcinogenic, and environmentally hazardous [13,14]. In addition to that, hydrazine is a volatile compound that requires rigorous safety protocols. The vapor of pure hydrazine may explode if ignited and incompatible with several materials, including many plastics and metals [15-17], which contrast with environmentally friendly and challenging to make a large production scale. So far, only a few works reported the non-hydrazine CZTSe synthesis, such as selenourea, sodium selenite, and selenium dioxide [18-20]; however, such reagents show several disadvantages. Selenourea can be dissolved in the water, but it is almost twenty times more expensive than sodium selenite or selenium in pellet form. On the other hand, sodium selenite is cheaper than selenourea, but it cannot easily make some reactions with Cu^{2+}, Zn^{2+}, and Sn^{4+} as the selenium in sodium selenite has selenium with a 4+ charge unless a strong reducing agent such as pyridine added into the solution, which can change Se^{4+} to Se^{2-}. Pyridine is suitable for the solution technique due to non or less carbon content, non-metal content and can easily mix with Cu, Zn, and Sn [21-23]. Nonetheless, pyridine is challenging

due to being a toxic, flammable, irritant, and carcinogenic agent [24-26]. In this work, CZTSe absorber layer was synthesized by two steps solution process. The first step was making CZT precursor from Cu, Zn, and Sn salts by utilizing monoethanolamine as chelating agent and solvent simultaneously. And the second step was selenization by Se elements under argon and hydrogen mixture gas.

Hence, this study primarily focuses on a novel non-hydrazine, low-cost, and environmentally friendly two-step solution process technique to synthesize high-quality CZTSe thin films. The film formation, reaction mechanism, chemical composition, and optoelectronic properties of CZTSe thin-film are systematically investigated in the current study. Next, the experimentally realized optical and electrical properties of deposited films are used to study CZTSe solar cells' photovoltaic properties by numerical simulations. The electrical characteristics of solar cells are examined by SCAPS simulations, where the optics and optimization of the device are investigated by finite-difference time-domain (FDTD) simulations in three dimensions [27-28]. Detailed discussions of the film preparation provided in the following sections. A detailed experimental description of film preparation and material characterization is presented in Section 2. Investigated results from the experiment and simulation are discussed in Section 3. The manuscript is summarized in Section 4.

2. Experimental Details

2.1. Soda-lime glass (SLG) preparation

Soda-lime glass (SLG) was cleaned by an ultrasonic water bath in acetone, ethanol, and deionized water for 20 minutes, respectively.

2.2. Preparation of CZT (Cu, Zn, Sn) Film Precursor

The CZT (Cu, Zn, and Sn) film precursor was made from annealed CZT solution precursor

prepared from Cu^{2+}, Zn^{2+}, and Sn^{4+} metal salts such as copper (II) acetate monohydrate, zinc acetate dihydrate, and tin (IV) chloride dihydrate were purchased from Sigma Aldrich. All metal salts were separately dissolved by ultrasonic-assisted in 10 mL ethanolamine, which was also purchased from Sigma Aldrich with the concentration of Cu, Zn, and Sn elements were 0.075 M, 0.050 M, and 0.050 M, respectively. After each metal salts were dissolved entirely in monoethanolamine (MEA), all those solutions were mixed until the solution's color was a dark blue. Then, ethanol was added until the solution's volume was 100 mL and stirred until homogeneous. The CZT precursor solution was later deposited using spin coating at 2000 rpm for 15 seconds on 2.5 cm x 2.5 cm soda-lime glass (SLG). Finally, it was annealed under an ambient atmosphere at 200 °C for 10 minutes in the tubular heater until black-brownish film color was obtained.

2.3. Growth of CZTSe Thin-film

The CZTSe thin films obtained by adding selenium into the CZT precursor through selenization under Ar (95%) and H_2 (5%) mix gases at 550 ^oC for 120 minutes with 10 sccm of flow rate. After selenization, the sample was cooled to room temperature under natural conditions.

2.4. Characterization of CZTSe Thin-film

The microstructural and cross-sectional analysis of films were determined under the scanning electron microscope (SEM) by Hitachi (S 4800, Japan), with an operating voltage of 15 kV. The compositional analysis of films was examined using the energy dispersive x-ray (EDX) by Horiba, Japan, attached to the respective SEM apparatus with an acceleration voltage, working distance, and emission current of 15 kV, 15 mm, and 10 μA, respectively. The crystallinity and structural analysis performed under an x-ray diffractometer (XRD) by Rigaku (DMAX 2500, Japan) with fixed angle 2θ, and λ = 1.5405 Å. The measurement conditions

were performed at 40 kV, 100 mA, scan speed 2θ with diffraction angle 2θ between 1° and 65°. The complimentary XRD data was obtained by Renishaw (REO2, U.K.) micro-Raman spectroscopy at 514.5 nm using Ar ion C.W. laser. The spectra absorption was recorded by Varian (Carry 5000, USA) UV-Vis-NIR Spectrophotometer in the wavelength range 300 - 1500 nm. Electrical properties were determined by Ecopia (HMS-300, USA) Hall-Effect measurement at 0.01 μA. The thermal study of CZT precursor and organic compound decomposition were characterized by differential scanning calorimetry (Q200, USA) supported with Fourier transform infra-red (FTIR) data by Perkin Elmer (C86199, USA).

3. Results and Discussion

The current study aims to prepare a high-quality CZTSe thin film for efficient photovoltaic applications. In the first part of this study, a two-step reaction method was used to fabricate the CZTSe thin films on the glass substrates, further characterized by essential techniques to confirm the high-quality film. The second part investigates the optoelectronic properties of CZTSe solar cells by numerical simulations. Experimentally realized optical and electronic values of the deposited CZTSe thin film were used as inputs for the numerical device modeling and simulations. More details on the investigations are provided in the following sections.

3.1. Realization of CZTSe Thin-film

In the two-step method, the first step contributes to preparing a CZT solution precursor from Cu2+, Zn2+, and Sn4+ metal salts using monoethanolamine (MEA) ethanol as mixed solvents. At this point, MEA acts as a chelating agent / complexant [29] and making a coordination compound with Cu^{2+}, Zn^{2+}, and Sn^{4+} metal salts. The copper-monoethanolamine (Cu-MEA) complex compound exhibits a dark blue color solution, while zinc- and tin-MEA

complex compounds appear in a transparent solution. However, it is challenging to evaporate MEA due to the high surface tension attached to the substrate. In order to reduce MEA's surface tension with increased wet ability, the metal-salt MEA complex compounds were mixed with ethanol until the metal-salt MEA to ethanol ratio reaches 30:70. The outcome is named the CZT precursor solution, which is stable due to forming a metal-salt MEA coordination compound with stronger bonding than metal-hydroxyl in ethanol. **Figure 1(a)** shows such a coordination mechanism. The chemical composition of the CZT solution was made with ratios of 0.75 and 1.00 for Cu/(Zn+Sn) and Zn/Sn conditions, respectively, which is the optimized condition to grow high-quality CZTSe thin film containing poor-copper zinc-rich at the final process [30-32].

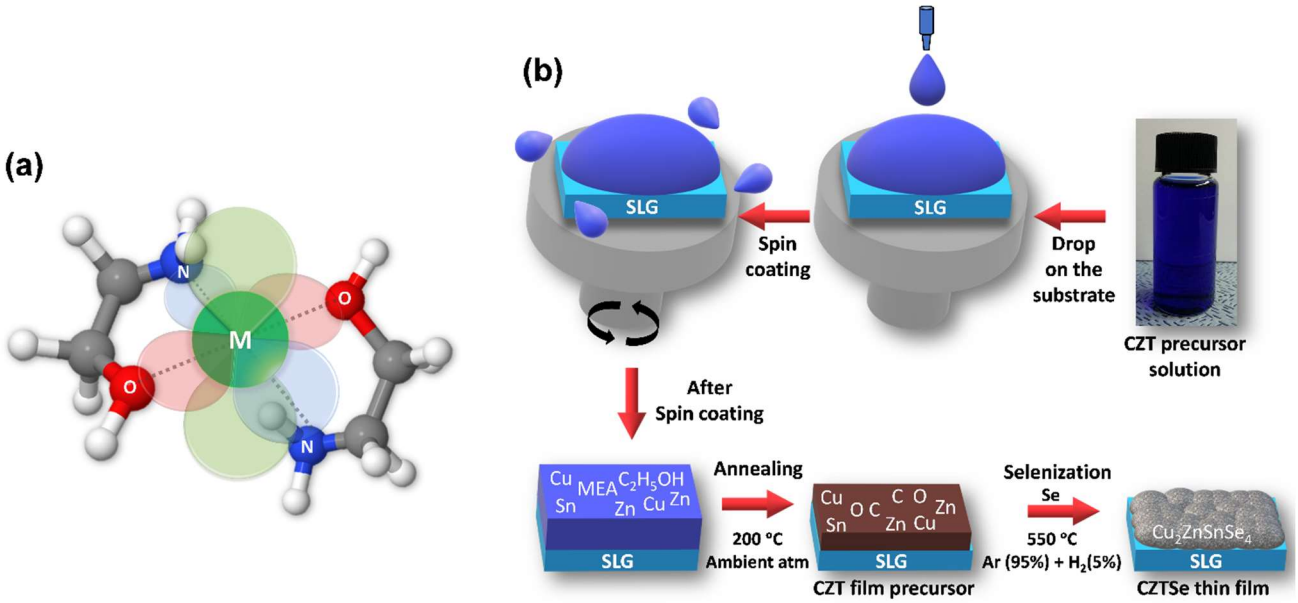

Figure 1. Schematic illustration of (a) the metal-monoethanolamine complex compound structure and (b) synthesizing CZTSe thin film from CZT precursor.

A detailed schematic illustration of the CZTSe film deposition from the CZT precursor solution is shown in **Figure 1(b)**, including both annealing and salinization processes. Firstly, in the preparation process, the CZT precursor solution was deposited onto SLG by spin coating at

2000 rpm for 15 secs, followed by a 15 mins annealing at 200 °C. During this step, metal-ethanolamine complex compounds were slightly decomposed, where intermetallic atoms make a binary alloy. In contrast, organic compounds, such as acetate, ethanol, and ethanolamine, decompose partially into organic residues (e.g., C or C.O.) as amorphous substances deposited along with Cu and intermetallic binary alloy.

The reaction of Cu, Zn, and Sn in the metal salts with MEA until the annealing process are:

$$M^{x+}\ (aq) + MEA\ (l) \rightarrow M[MEA]_x\ (aq) \quad (1)$$

$$M[MEA]_x\ (aq) \rightarrow M\ (s) + Organic\ residue\ (s) \quad (2)$$

$$Cu\ (s) + Zn\ (s) \rightarrow Cu_xZn_y\ (s) \quad (3)$$

$$Cu\ (s) + Sn\ (s) \rightarrow Cu_xSn_y\ (s) \quad (4)$$

where, M = Cu, Zn, and Sn.

3.1.1. *Structural and Surface Properties of CZTSe Thin-film*

The resulting XRD pattern of the annealed CZT precursor film is shown in **Figure 2**, showing two diffraction peaks at 2θ= 43.3° and 50.4° that are assigned to (111) and (200) planes, respectively. Such peaks probably appear from copper and intermetallic binary alloy, e.g., Cu_xZn_y and Cu_xSn_y, surrounded by organic amorphous residue, shown as a broad 2θ peak below 35°. Possibly, both intermetallic compounds may form below 200 °C according to Cu, Zn, and Sn ternary phase diagram. However, there was no evidence for the Zn_xSn_y compound or even metal oxide from the metal-MEA complex compound due to the preferential reaction between zinc and tin with copper. The initial chemical composition of the CZT precursor is also similar to the result published by Wibowo *et* al. in the literature [33]. In this study, the chemical composition of Cu, Zn, and Sn was maintained to 45%, 30%, and 25%, respectively, with the Cu/(Zn+Sn) ratio of 0.82 matching the XRD pattern with the Cu-Zn-Sn ternary phase diagram shown in **Figure 2(a)**. In addition to inorganic compounds, this work also involves organic compounds, such as acetate from metal salts, ethanol, and MEA, as solvents that

can leave organic residue in the film as carbon or graphite. Fourier transform infra-red (FTIR) and Raman measurements will benefit from tracing such organic residues. The resultant spectrum of the CZT precursor before and after annealing from FTIR and Raman spectroscopy is presented in **Figures 2(b)** and **2(c)**, respectively. Figure 2(b), peaks at 1365 cm^{-1} and 1469 cm^{-1}, showed CH_2 and CH_3 group peaks in ethanol.

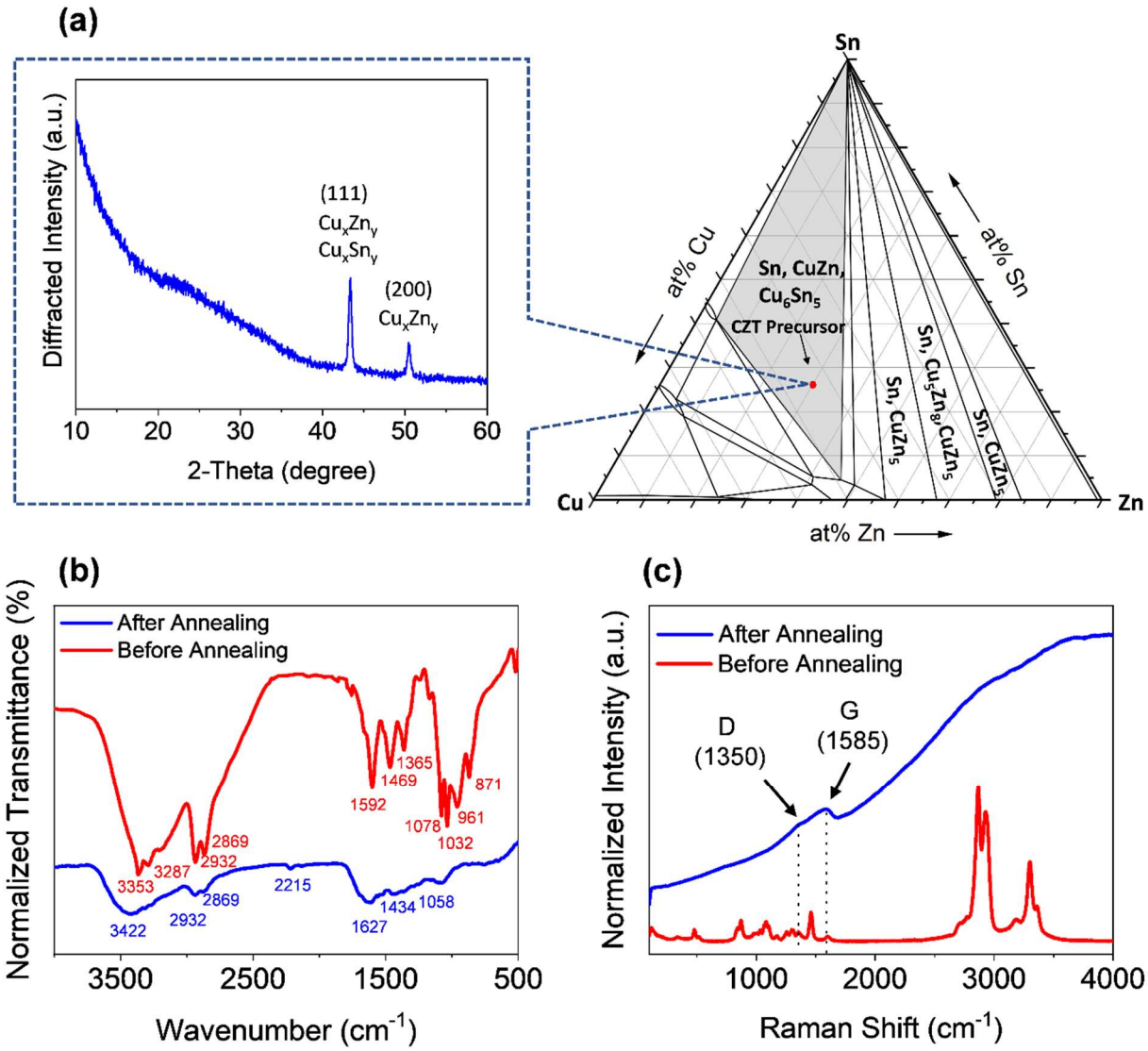

Figure 2. (a) XRD pattern of the annealed CZT precursor at particular composition in the Cu-Zn-Sn ternary phase diagram. (b) Fourier transform infrared (FTIR) spectrum and (c) Raman spectroscopy of CZT precursor before and after the annealing process.

However, besides showing a peak for the CH_3 group in the ethanol, the peak at 1469 cm^{-1} was also showing the CH_2 group in the ethanolamine. A broad peak at 3353 cm^{-1} shows

hydroxyl influenced by hydrogen bonding from the solvent. Peaks at 3287 cm^{-1}, 1078 cm^{-1}, 1032 cm^{-1}, and 1592 cm^{-1} belong to N-H. However, this peak is a specific indication of the aliphatic amine group. The exhibited peaks at 2932 cm^{-1} and 2869 cm^{-1} confirm the hydrocarbon (C-H) bonding. Overall, the spectrum of CZT precursors in the solution phase was dominated by the ethanolamine spectrum due to ethanol had a similar molecule with ethanolamine. Therefore, ethanol peaks were covered by ethanolamine peaks. After annealing, the CZT precursor shows a different spectrum from the CZT precursor in the solution phase, which could be shifted, decreased the intensity, or even disappeared. These conditions are evidence that organic compounds in the CZT precursor were decomposed partially. However, the MEA has amine and hydroxyl as active sites, and both sites could react with some compounds during calcination that can be identified as the broad peak at 3422 cm^{-1}, which exhibit for hydroxyl site (-OH) from ester without hydrogen bonding between ligand and solvent, peak at 2215 cm^{-1} was specifically represented nitrile group, peaks at 2932 cm^{-1} and 2869 cm^{-1} represent C-H bonding that is still existing even after annealing.

Furthermore, shoulder peaks at 1700 cm^{-1} and 1627 cm^{-1} show the C=O bonding and N-H group, respectively. Nevertheless, after calcination, the CZT precursor condition is sufficient to prevent oxidation in the CZT film precursor due to oxidation in the ligand. This result was consistent with TGA-DSC data, which shows dihydroxylation and decomposition partially in the CZT precursor thin film. On the other hand, **Figure 2(c)** reveals Raman spectra for the CZT film before the annealing process, exhibiting specificity for the Cu, Zn, and Sn salts in the MEA. However, after annealing, Raman spectra completely changed that exhibits D and G peaks at 1350 cm^{-1} and 1585 cm^{-1}, respectively. Clearly, almost every organic compound has decomposed into carbon that majority as graphite compound showing a specific pattern for the Cu, Zn, and Sn salts in the MEA.

The thermal properties of the CZT precursor were studied by thermal gravimetry – differential scanning calorimetry (TG-DSC); results are shown in **Figure 3(a)**. When the temperature exceeded 200 °C, the T.G. graphic shows a significant decrease up to 400 °C. This phenomenon indicates further decomposition of organic residues and the rest of the organic compounds. From its derivative weight could be seen the decomposition by a high derivative of weight from 200 °C to 500 °C. On the other hand, the DSC curve also clearly seen the decomposition phenomenon showing a significant decreasing trend or endothermic trend from 400 to 600 °C.

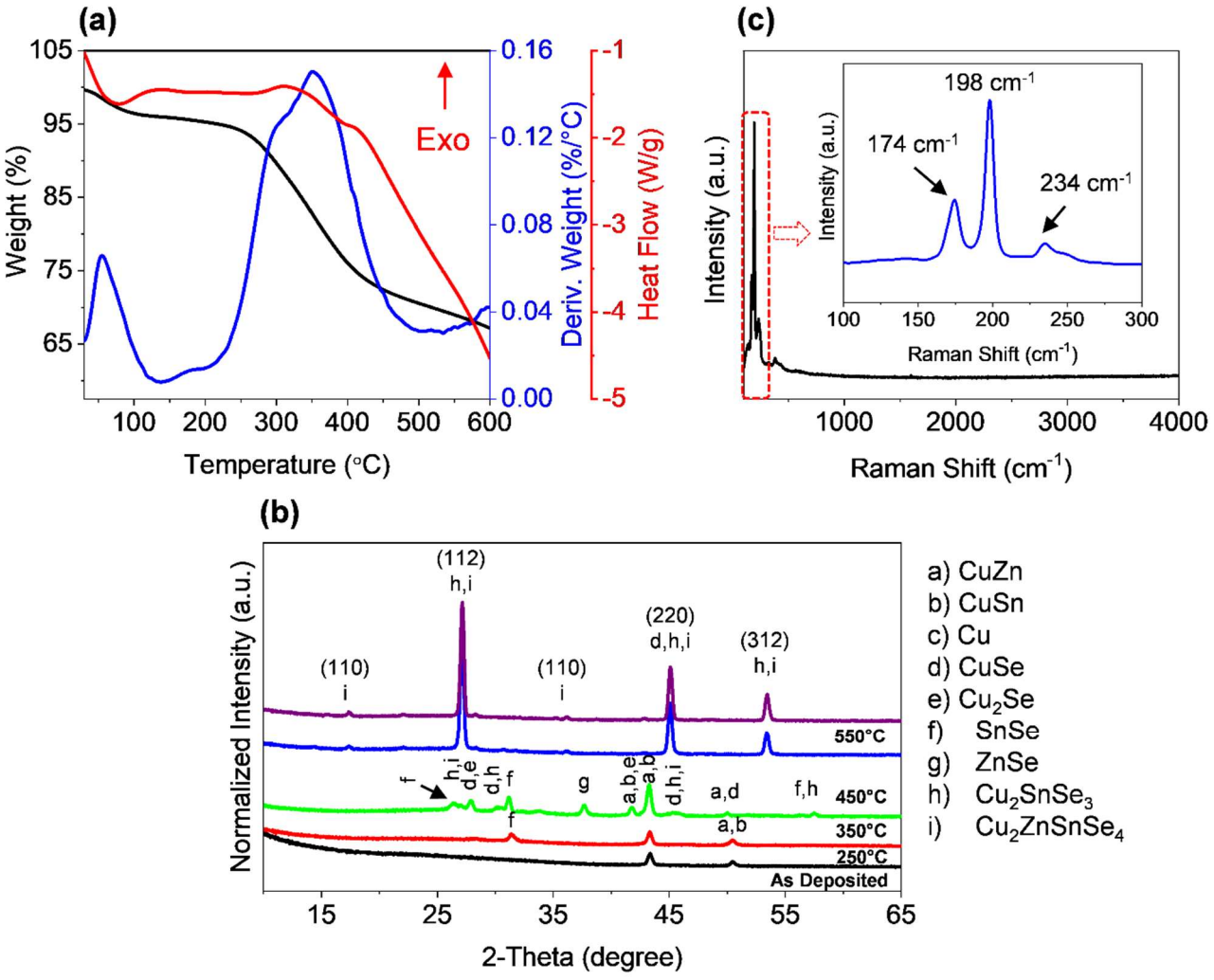

Figure 3. (a) TGA-DSC graphic of CZT precursor at 27 °C – 500 °C. (b) XRD pattern of CZT precursors at elevated selenization temperatures under Ar (95%) + H_2 (5%) for 120 min. (c) Raman spectrum of CZTSe thin film. Inset shows the expanded view of Raman shift for 100 to 300 cm^{-1}.

However, from 300 to 350 °C, it shows a slight exothermic peak which corresponds to binary alloy formation such as CuZn and CuSn. The partial decomposition phenomenon of the CZT precursor also is confirmed by FTIR characterization in **Figure 2(b)**, indicating the thin film was shrinking due to releasing some organic residues. **Figure 3(a)** shows the TGA-DSC graphic of the CZT precursor for the temperature ranging from 27 °C to 500 °C under ambient atmosphere. The XRD pattern of CZT precursors at elevated selenization temperature is shown in **Figure 3(b)**. In the selenization process at 250 °C, the CZT precursor was reacted with selenium, which already evaporated in small amounts to form SnSe, which marked as a peak at 2θ = 31.37° and also probably there was CuSe which marked on a small peak at 2θ = 25.63°. Besides, CuSe and SnSe, at this condition, also form Cu_xZn_y and Cu_xSn_y binary alloy due to still dominant compounds at this moment. At 350 °C, not only binary and ternary compounds occurred, but there are also quaternary compounds. Binary compounds that occurred are CuSe, Cu_2-Se_x, SnSe. Besides, there is a formation of ternary and quaternary compounds $CuSnSe_3$ and $Cu_2ZnSnSe_4$, respectively. At 450 °C and 550 °C, there are five peaks at 2θ = 17.35°, 27.13°, 36.11°, 45.09°, and 53.45° which can be indexed to (101), (112), (211), (204/220), and (312/116) respectively. These peaks are probably belong to Cu_2SnSe_3 (ICDD: 01-089-1879) or $Cu_2ZnSnSe_4$ peaks (ICDD: 00-052-0868). In XRD, the difficulty lies in the presence of a secondary phase such as Cu_2SnSe_3 (CTS), which has the same underlying zinc-blende structure (when neglecting the difference between cations) as kesterite or stannite phases of CZTSe. All of these reactions were described in **Figure 3(b)**. The CZT precursor's reactions involved several reactions that could be divided into primary, binary, ternary, and quaternary reactions. The primary reaction occurs between Se and H_2, Cu, Zn, and Sn, producing binary compounds, such as H_2Se, Cu_xSe, ZnSe, and SnSe. The binary reaction happens because some binary compounds, such as Cu_xSe, ZnSe, SnSe,

CuZn, and CuSn, react with H_2Se form a Cu_2SnSe_3 (CTS) as a ternary compound. The ternary compound (CTS) reacts with ZnSe, which leads to the quaternary reaction. All these reactions are provided in the following.

Primary reactions:

$$Se\ (g) + H_2\ (g) \rightarrow H_2Se\ (g) \quad (5)$$

$$Cu\ (s) + H_2Se\ (g) \rightarrow Cu_xSe\ (s) + H_2\ (g) \quad (6)$$

$$Zn\ (s) + H_2Se\ (g) \rightarrow ZnSe\ (s) + H_2\ (g) \quad (7)$$

$$Sn\ (s) + H_2Se\ (g) \rightarrow SnSe\ (s) + H_2\ (g) \quad (8)$$

$$C\ (s) + H_2\ (g) \rightarrow CH_x\ (g) \quad (9)$$

Binary reaction:

$$CO\ (s) + H_2\ (g) \rightarrow CH_x\ (g) + H_2O\ (g) \quad (10)$$

$$CuZn\ (s) + H_2Se\ (g) \rightarrow Cu_xSe\ (s) + ZnSe\ (s) + H_2\ (g) \quad (11)$$

$$CuSn\ (s) + H_2Se\ (g) \rightarrow Cu_xSe\ (s) + SnSe\ (s) + H_2\ (g) \quad (12)$$

Tertiary reactions:

$$CuSe\ (s) + CuSn\ (s) + 2\ H_2Se\ (g) \rightarrow Cu_2SnSe_3\ (s) + 2\ H_2\ (g) \quad (13)$$

$$Cu_2Se\ (s) + SnSe\ (s) + H_2Se\ (g) \rightarrow Cu_2SnSe_3\ (s) + H_2\ (g) \quad (14)$$

$$CuSn\ (s) + H_2Se\ (g) \rightarrow Cu_2SnSe_3\ (s) + H_2\ (g) \quad (15)$$

Quaternary reaction:

$$Cu_2SnSe_3\ (s) + ZnSe\ (s) \rightarrow Cu_2ZnSnSe_4\ (s) \quad (16)$$

The Raman spectra confirm the CZTSe thin films' formation, while selenization temperature altered from 250 °C to 550 °C, leading to the existence of carbon in the film. Initially, no peak

was observed in the case of CZT precursor; however, at 250 ºC, a peak has appeared at 258 cm^{-1}, which belongs to the CuSe or Cu_2Se compound and products of a reaction between copper in the CZT precursor and selenium in the atmosphere at 250 °C and 350 ºC, respectively. The CZTSe peak started to occur at 198 cm^{-1} with 450 °C while Raman spectra also exhibit organic residue in carbon compounds as amorphous carbon. It resulted in a spectrum with a slope and marked as a specific peaks pattern named D and G peaks at 1350 cm^{-1} and 1585 cm^{-1}, respectively. Exhibited Raman spectra (D and G peaks) disappeared gradually with the elevated temperature. Finally, at 550 °C, Raman spectra reveal specific peaks for CZTSe at 174 cm^{-1}, 198 cm^{-1}, and 234 cm^{-1} without showing D and G peaks, as shown in **Figure 3(c)**. Raman spectra for CZTSe confirmation peaks and carbon residue are shown in **Figure S1** and **Figure S2**, respectively, in the Supporting Information.

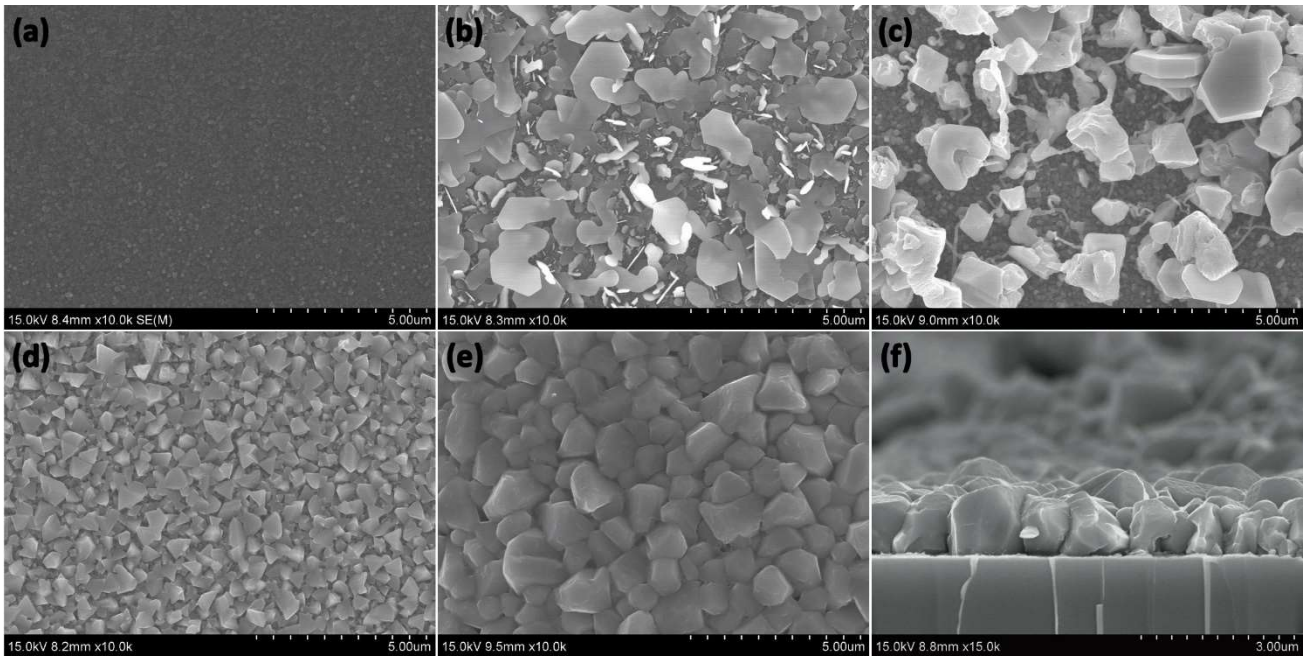

Figure 4. SEM images of (a) CZT precursor, (b) CZT precursor while selenization at 250 °C, (c) 350 °C, (d) 450 °C, and (e) 550 °C and (f) it's cross-section, under Ar (95%) + H_2 (5%) atmosphere for 120 min.

The surface and cross-sectional morphologies of the CZT precursor film are shown in **Figure 4**, exhibiting a small grain. At 250 °C, the hexagonal shape indicates the presence of copper

selenium (Cu_2-Se_x) compound and the formation of a small amount of SnSe. In the case of 350 °C selenization, selenium binary compounds, such as CuSe, ZnSe, and SnSe, are observed, which show hexagonal, tetragonal, and thread-like shape, respectively, as shown in **Figure 4(c)**. SEM images are also consistent with the previously studied XRD pattern and Raman spectrum. Although, 450 °C case offers a small grain size of CZTSe; nevertheless, grain size is greatly increased at the elevated temperature (550 °C), forming the CZTSe film with high crystallinity. At 550 °C, CZTSe has a granular and compact shape with a thickness of approximately 1300 nm. This result is also consistent with the Raman spectrum result for elevated selenization temperature at 450 °C and 550 °C.

9 The chemical composition of CZTSe films was determined by the energy-dispersive x-ray spectroscopy (EDX) with different selenization temperatures. At elevated temperatures, the amount of selenium increased due to the compound containing selenium, starting from primary, binary, tertiary, and finally, a quaternary compound. In addition to that, some elements (e.g., Sn) may be evaporated during the selenization process, which leads to a change in the film's chemical composition. **Figure S3** and **Table S1** in the Supporting Information present the changing of chemical composition while varying the selenization temperatures. The determination of chemical composition uses a comparison of each element's intensity in the sample; for example, if the selenium amount in the sample increases, the other components should be decreased. Hence, the chemical composition ratio was taken under consideration in the current study. We used the component ratio (Cu/(Zn+Sn), Zn/Sn, and Se/metal) approach to describe chemical composition in the thin film. This information helps to know the change for tin and selenium in the film. Thus, Cu/Zn and Cu/Sn ratio should be calculated to describe the change in Cu and Zn during the selenization process.

3.1.2. *Optoelectronic Properties of CZTSe Thin-film*

The UV-vis measurements allow determining the transmittance and absorption of the fabricated CZTSe thin-film, which further allows calculating essential optical parameters, such as complex refractive index, absorption coefficient, extinction coefficient, and bandgap of the prepared film. **Figure 5(a)** demonstrates the wavelength-dependent transmittance for different selenization temperatures, where it is clearly understood that the fabricated CZTSe thin-film has a high transmission (~80%) for the longer wavelength (>900 nm) while exhibiting high absorbance (almost no transmission) from visible to the near-infrared regions, as shown in **Figure S4**. An Image of CZT precursor before and after selenization process is provided in **Figure S5** in the Supporting Information. Such optical phenomena are infrequent in the case of CZTSe film, which confirms the effective film deposition and prospects for making CZTSe solar cells with high efficiency.

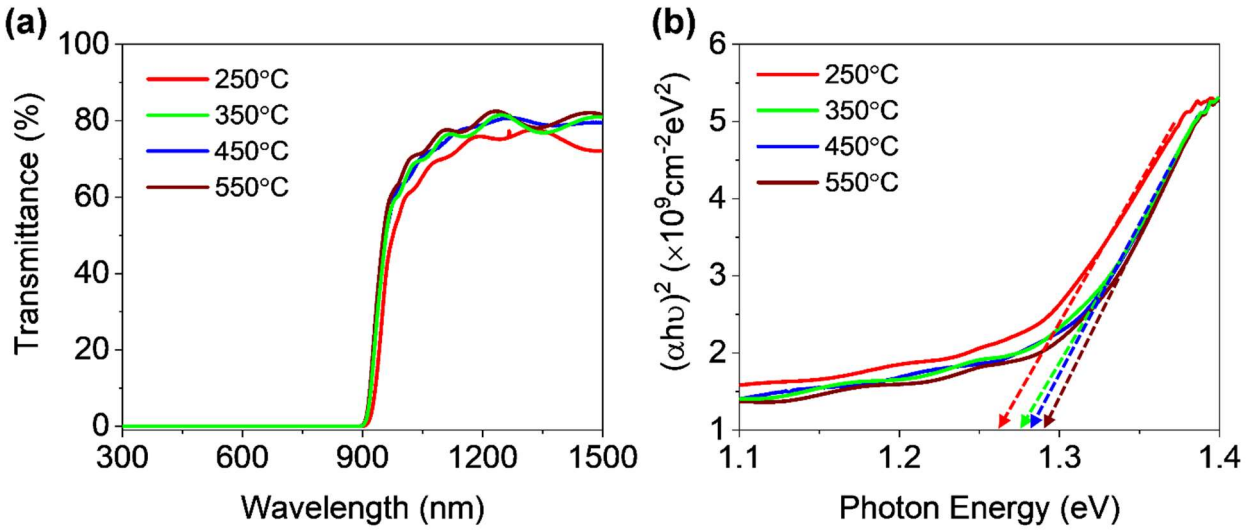

Figure 5. (a) Transmittance and (b) Tauc plot for determining the direct optical band gap of CZTSe film. The film was annealed at 250 °C to 550 °C for 120 minutes under Ar (95%) + H_2 (95%) atmosphere.

Figure 5(b) shows the Tauc plot for determining bandgaps while varying the film's salinization temperature. The bandgap of the fabricated CZTSe film is calculated to 1.26 eV, 1.27 eV,

1.28 eV, and 1.29 eV for salinization temperature of 250 °C, 350 °C, 450 °C, and 550 °C, respectively. The realized band gaps are very suitable for the realization of efficient CZTSe solar cells. The electrical properties, such as carrier concentration, carrier mobility, conductivity, and resistivity, of the deposited CZTSe thin-film were determined using the Hall measurement. It has been found that the electrical properties are mostly influenced by the organic and inorganic phases of the film.

Table 2. Electrical properties of CZT precursor at elevated selenization temperature under Ar (95%) + H_2 (5%) for 120 min.

Temp (°C)	Carrier Concentration (cm^3)	Mobility (cm^2/Vs)	Resistivity (Ω-cm)
250	1.72×10^{11}	1.28×10^{-6}	2.55×10^{1}
350	5.70×10^{15}	4.30×10^{-5}	3.25×10^{0}
450	8.26×10^{17}	1.05×10^{0}	3.40×10^{-2}
550	1.75×10^{18}	3.20×10^{0}	6.48×10^{-2}

In the case of 250 °C, the thin film is dominated by organic residues and still, having a low content of metal selenide compounds. CZTSe has both low carrier concentration and mobility; and exhibits a high resistivity due to carbon residue that acts as an insulator. Furthermore, at elevated temperature, both carrier concentration and mobility gradually increased; yet, resistivity gradually decreased because, at 350 to 450 °C, binary and ternary compounds start to form, whereas carbon residue slowly disappeared. Finally, at 550 °C, CZTSe has been wholly developed without showing any secondary and ternary phases. Measured carrier concentration, mobility, and resistivity of CZTSe at elevated temperature are shown in **Table 2**.

3.2. Examining Optoelectrical properties of CZTSe thin film by device modelling

The investigated CZTSe thin-film exhibits excellent optoelectronic properties, which is very much suitable for realizing efficient solar cells. The experimental findings from fabricated CZTSe thin-film are comparable to the literature's best results [33,34]. In this part of the study, we have designed and modelled a CZTSe solar cell based on the experimental properties of this study. Later, we have investigated the photovoltaic properties of proposed CZTSe solar cell and compared with the reported literatures. In the first step, we utilized the Solar Cell Capacitance Simulator (SCAPS-1D) to study the planar CZTSe solar cell [36, 37]. SCAPS characterizes the solar cell performance parameters in one dimension; however, as we deal with only the planar structure, the solver is able to provide reasonable estimation while considering possible assumptions.

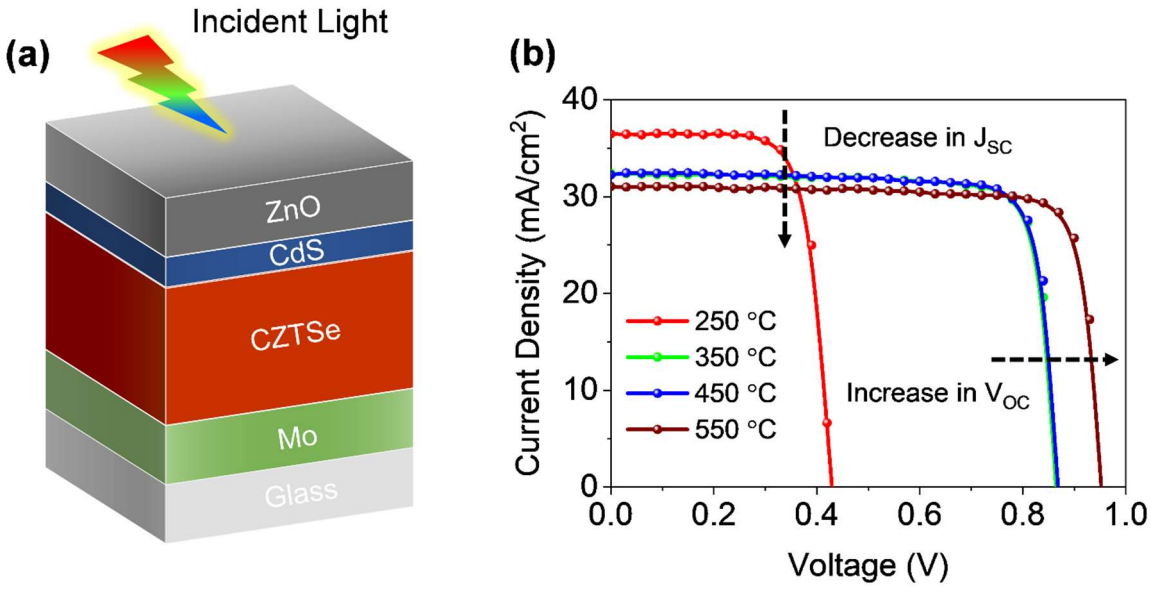

Figure 5. (a) Schematic diagram of the studied CZTSe solar cell. (b) A comparison of CZTSe solar cells' J-V characteristics for different selenization temperatures while preparing the CZTSe thin films.

The simulation offers current-voltage (JV) characteristics of solar cells, and later, photovoltaic performance parameters can be extracted. More details of the SCAPS-1D electrical simulation method are provided in Section **S1** of the Supporting Information. In this method,

experimentally realized electronic parameter values were used as inputs. **Figure 6(a)** depicts the schematic diagram of the investigated CZTSe solar cell, where the simulation's input material properties are given in **Tables 3, 4,** and **5**. A substrate type configuration was considered for designing the solar cell. The CZTSe absorber is placed on top of the thick Mo coated glass substrate, followed by 100 nm CdS and 80 nm ZnO layers, where the incident light hits the ZnO layer first, then propagates to the bulk of the device.

Table 3. Material Properties Used for simulations.

Parameters	***ZnO* [39]**	***CZTSe* [38,41]**	***CdS* [40]**
Thickness (nm)	80	1500	100
E_g (eV)	3.3	Experiment (1.26~1.29 eV)	2.4
χ (eV)	4.4	4.55-4.49	4.2
ε_r	9	9.4	10
Nc (cm^{-3})	2.5×10^{18}	2.2×10^{18}	2.2×10^{18}
Nv (cm^{-3})	2.0×10^{19}	1.5×10^{19}	1.8×10^{19}
μ_e (cm^2/Vs)	100	100	100
μ_h (cm^2/Vs)	25	12.5	25
N_D (cm^{-3})	1.0×10^{18}	-	1.5×10^{17}
N_A (cm^{-3})	-	Experiment	-

Table 4: Device parameters used in the simulation.

Simulated Cell Properties	
Cell temperature	300 K
Series resistance R_s	4.25 Ωcm^2
Shunt Resistance R_{sh}	370 Ωcm^2

Table 5. Contact material properties used in the simulation.

Contact Material Properties			
Property	**Front contact**	**Back contact**	
Surface recombination velocity of electron	10^7 cm/s	10^5 cm/s	10^5 cm/s
Surface recombination velocity of hole	10^5 cm/s	10^7 cm/s	10^7 cm/s
Metal work function	Flat band	Flat band	Mo (5 eV)

As shown in **Figure 5(b),** simulated J-V curves reveal that J_{SC} of the solar cell gradually decreases with the increase in temperature. In contrast, the V_{OC} of the solar cell has increased. It is evident that the annealing temperature of the CZTSe film preparation has not only to influence the film properties but also effects the optoelectronic properties of CZTSe solar cells. We revealed that Voc has increased due to two factors: change in bandgap and change in carrier concentration. In this experiment, bandgap of CZTSe has increased with the annealing temperature which attributed to increase in Voc and decrease in Jsc. Again, Voc has a significant relation with carrier concertation which is expressed in equation 17:

$$v_{oc} = \frac{kT}{q} ln\left[\frac{(N_A+\Delta n)\Delta n}{n_i^2}\right] \quad (17)$$

where kT/q is the thermal voltage, N_A is the doner concentration, Δn is the excess carrier concentration and n_i is the intrinsic carrier concentration. It determines that Voc increases with the increase of donor concentration while other factors are constant. In our experiment we observed that CZTSe carrier concentration has increased with the increase of annealing temperature, that also contributed to increase of Voc of the device. The J_{SC} and V_{OC} varied from 36.5 to 31.5 mA/cm^2 and 0.42 to 0.95 V, while ranging the CZTSe film's annealed temperature from 250 to 550°C, respectively. Hence, an optimization is required to maintain the trade-off between photovoltaic parameters. The temperature-dependent J_{SC}s and V_{OC}s of simulated CZTSe solar cells are demonstrated in **Figure S6,** along with the bandgaps of annealed CZTSe thin-films. It has been discovered that the CZTSe film has to be annealed at approximately 360°C to achieve the optimum point. V_{OC} and J_{SC} are around 0.75 V and 34.8 mA/cm^2, respectively, at the optimum point, which has a fill-factor (FF) of ~82%. The CZTSe bandgap of the optimized solar cell is nearly 1.27 eV (**Figure S6**), theoretically, which can absorb photons up to ~980 nm incident wavelength. Therefore, an estimated PCE of the optimized CZTSe solar cell can go up to 21.4%.

However, 1D numerical simulations are mostly limited to provide a complete understanding

of underlying device optics. The optics of solar cell has a great influence on the solar cell's efficiency. To determine the realistic photovoltaic performance, it is essential to investigate the optical wave phenomena within a solar cell structure in three dimensions (3D) [42,43]. Hence, as a second step, 3D finite-difference time-domain (FDTD) optical simulations were carried out to study solar cells' electromagnetic wave propagation and optical characteristics [27]. The optimized device structure was considered for the optical simulation, where complex refractive indices derived from the optical investigation of materials were used as input parameters. The optical wave propagation for the device was modeled from 300 to 1000 nm wavelength close to the fabricated CZTSe absorber bandgap (~1.27 eV). The incident plane wave is circularly polarized, which has an amplitude of 1 V/m. The FDTD simulation results in electromagnetic field distribution within the solar cell, further enabling the calculation of power density, quantum efficiency (QE), and J_{SC} of the solar cell [28]. A detailed discussion on power density, QE, and J_{SC} calculation is provided in the Supporting Information (Section **S2**). Furthermore, the maximum value of the collection efficiency is expected to be unity.

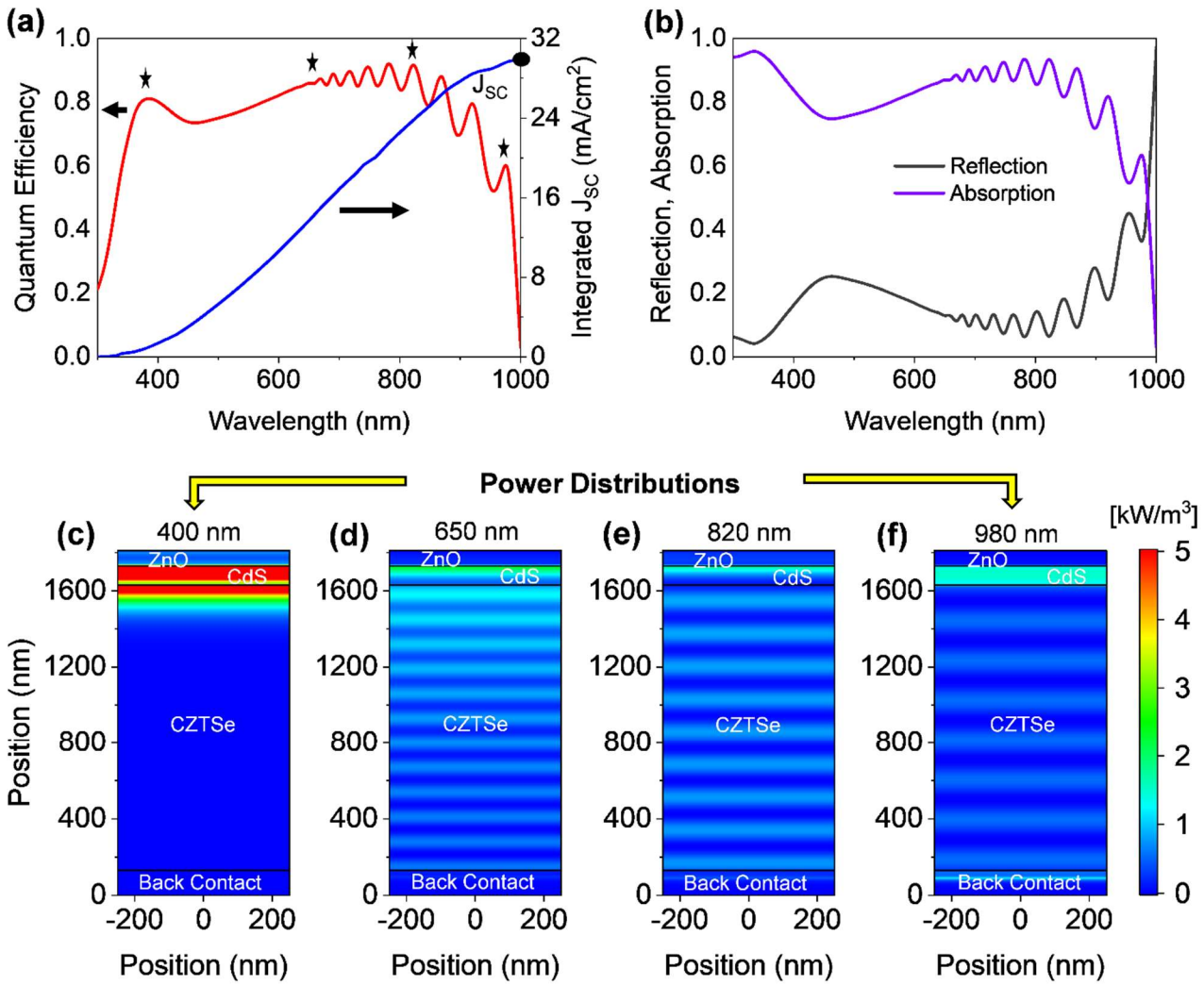

Figure 7: Simulated (a) QE and integrated J_{SC}, (b) absorption and reflection of the CZTSe solar cell. A cross-sectional power density maps of the investigated solar cell under monochromatic illumination of (c) 400 nm, (d) 650 nm, (e) 820 nm, and (f) 980 nm, respectively.

Figure 7(a) shows the calculated QE and corresponding integrated J_{SC} of the investigated CZTSe solar cell. The QE reveals a larger variation throughout the whole spectrum, and photons are absorbed up to 1000 nm, which nicely matches the theoretical estimation from the realized CZTSe bandgap. However, the J_{SC} of the solar cell is calculated to 30 mA/cm^2, which is almost 5 mA/cm^2 lower than the estimated J_{SC} from the 1D simulation; nevertheless, such a discrepancy is acceptable for the study as the optical simulation considers a 3D environment. As compared to the shorter wavelengths, QE in the longer wavelengths exhibits

a higher number of interference fringes, which is due to several forward and backward wave propagations in the more extended wavelength region. The optical phenomena can be further confirmed by the simulated power density profiles for incident wavelengths of 400 nm, 650 nm, 820 nm, and 980 nm are shown in **Figure 7(c-f)**. The CZTSe has a higher absorption coefficient at the shorter wavelengths; hence, photon absorptions are much higher in the shorter wavelength region. However, for the shorter wavelength (<400 nm), as shown in **Figure 7(d)**, most incident photons are either absorbed by the contact to buffer layers or CdS/ CZTSe interface, where photons travel to a few hundred nanometers of the CZTSe layer. With increasing the wavelength (650 nm), the absorption in the absorber layer is also increased shown in **Figure 7(e)**. However, a further increase in wavelengths (**Figure 7(e)**) lead to limit the QE due to several constructive and destructive interferences. At 980 nm, photon absorption in the device is almost zero, which is due to the material properties the deposited CZTSe film, close to the bandgap; nonetheless, a fraction of photons is considered as a loss that is due to the plasmonic effects at the metal/semiconductor interface, as shown in **Figure 7(f)**. The investigated solar cell's electrical field distribution profiles are provided in **Figure S7** in the Supporting Information, which can further validate the optical wave propagation in the device. The investigated solar cell pronounces higher reflections due to the planar front surface that restricts the total photon absorption in a solar cell and does not contribute to the QE, JSC, and PCE, as shown in **Figure 7(b)**. By texturing the surface or solar cell's interfaces, photon absorptions can be improved; however, this is not a scope of this current study. We limited our study to study the optoelectronic characteristics of a basic CZTSe solar cell to realize our fabricated thin-film's potential as an absorber. The CZTSe solar cell's realistic PCE can be estimated to ~18.5%, which can exhibit a J_{SC} of 30 mA/cm^2, V_{OC} of 0.75 V, and FF of 82%.

Table 6: Comparison of photovoltaic performance of CZTSe solar cells.

Cell Structure	*Voc (V)*	*Jsc (mAcm^{-2})*	*FF (%)*	*PCE (%)*	*Year*	*Ref.*
CZTSe/CdS	0.513	35.2	69.8	12.6	2014	[42]
CZTSe/CdS	0.41	37.27	73.79	11.43	2019	[43]
CZTSe/CdS	0.38	35.36	59.9	8.2	2016	[44]
CZTSe/CdS	0.75	30	82	**18.5**	2021	**This Study**

To provide further context, we compared our investigated CZTSe solar performance with recently published best CZTSe solar cells, which are listed in Table 6. Our findings reveal that the proposed CZTSe solar cell can outperform so far all characterized similar CZTSe solar cell performance and push forward to realize highly efficient CZTSe based photovoltaic devices.

4. Conclusions

In this study, $Cu_2ZnSnSe_4$ (CZTSe) thin-film has been prepared by a two-step reaction method from the CZT precursor, deposited from the metal-ethanolamine complex compound without hydrazine addition selenization. The deposited film's structural and optoelectronic properties were studied via necessary material characterization that confirmed the CZTSe film's high-quality, utilizing it as a photovoltaic absorber. It is found that the annealing temperature of the CZTSe film deposition has a great influence on its material properties. Organic impurities were disappeared gradually due to the effect of elevated temperature and atmospheric effect. It is noticed that the composition was changed at elevated selenization temperatures. However, organic impurities from organic residue were disappeared gradually under 450 °C. An increase in selenization temperature leads to an increase in the bandgap of the film. To confirm the potential of deposited CZTSe film, optical and electronic

characteristics of CZTSe-based solar cells were studied by electromagnetic numerical simulations. The SCAPS simulation tool investigated the J-V characteristics, where optics was examined by finite-difference time-domain (FDTD) optical simulations in 3D. The optimized bandgap of the CZTSe film is 1.27 eV, which allows realizing estimated PCE to 18.5% with a J_{SC} of 30 mA/cm^2, V_{OC} of 0.75 V, and FF of 82%. The proposed CZTSe solar cell can outperform all similar characterized best solar cells and provide a major breakthrough in CZTSe solar cells with high photovoltaic performance. A detailed investigation of the CZTSe film preparation and its application to photovoltaic technology is systematically discussed in the manuscript.

Competing interests

The authors declare no competing interests.

Supporting Information

Supplementary information is available from the authors.

Acknowledgments

This paper tributed to Prof. Kim Kyoo Ho as the author's supervisor (Ersan) in Yeungnam University for his kindness as the last paper before the retirement. This study was supported by the Basic Science Research Program (2013R1A1A2013408) and Center for Inorganic Photovoltaic Materials (No.2012-0001170) through the National Research Foundation of Korea (NRF) funded by the Ministry of Science, ICT and Future Planning. Authors also extended their appreciation to The University Researchers Supporting Project Number

(TURSP-2020/264), Taif University, Taif, Saudi Arabia. Thanks to the Ministry of Education and Culture of the Republic of Indonesia and all collaborators from the University of Indonesia and Kanazawa University, and The National University of Malaysia through the research grant support with code RS 2018-003. The authors gratefully acknowledge to Dr. Marc 394 Bargeman, University of Gent, Belgium, for providing the SCAPS simulation software.

References

[1] Yan, C., Huang, J., Sun, K., Johnston, S., Zhang, Y., Sun, H., ... & Yang, L. (2018). Cu 2 ZnSnS 4 solar cells with over 10% power conversion efficiency enabled by heterojunction heat treatment. Nature Energy, 3(9), 764-772.

[2] Zhang, Z., Gao, Q., Guo, J., Zhang, Y., Han, Y., Ao, J., ... & Zhang, Y. (2020). Over 10% Efficient Pure CZTSe Solar Cell Fabricated by Electrodeposition with Ge Doping. Solar RRL, 4(5), 2000059.

[3] Wang, W., Winkler, M. T., Gunawan, O., Gokmen, T., Todorov, T. K., Zhu, Y., & Mitzi, D. B. (2014). Device characteristics of CZTSSe thin-film solar cells with 12.6% efficiency. Advanced Energy Materials, 4(7), 1301465.

[4] David B. Mitzi, Oki Gunawan, Teodor K. Todorov, Kejia Wang, Supratik Guha. Solar Energy Materials and Solar Cells 95 (2011) 1421-1436.

[5] T.K. Todorov, J. Tang, S. Bag, O. Gunawan, T. Gokmen, Y.Zhu, D.B. Mitzi, Beyond 11% efficiency: characteristics of state-of-the-art $Cu_2ZnSn(S,Se)_4$ solar cells, Advanced Energy Materials 3 (2012) 34-38.

[6] Muslih, E. Y., & Kim, K. H. (2015). Characteristics of Cu2ZnSnS4 thin film prepared by calcination and sulfurizing of metal (Cu, Zn, Sn)-ethanolamine precursor complexed from metal (Cu, Zn, Sn)-hydrate. Chalcogenide Lett, 12, 349-355.

[7] Amal, M. I., & Kim, K. H. (2013). Structural and optical properties of sulfurized Cu 2

ZnSnS 4 thin films from Cu–Zn–Sn alloy precursors. Journal of Materials Science: Materials in Electronics, 24(2), 559-566.

[8] Munir, B., Prastyo, B. E., Muslih, E. Y., & Nurjaya, D. M. (2016). Non-sulfurization Single Solution Approach to Synthesize CZTS Thin Films. International Journal of Technology, 7(8), 1326-1334.

[9] Todorov, T., Kita, M., Carda, J., & Escribano, P. (2009). Cu2ZnSnS4 films deposited by a soft-chemistry method. Thin Solid Films, 517(7), 2541-2544.

[10] Sun, Y., Zhang, Y., Wang, H., Xie, M., Zong, K., Zheng, H., ... & Lau, W. (2013). Novel non-hydrazine solution processing of earth-abundant Cu 2 ZnSn (S, Se) 4 absorbers for thin-film solar cells. Journal of Materials Chemistry A, 1(23), 6880-6887.

[11] Y.E. Romanyuk, C.M. Fella, A.R. Uhl, M. Werner, A.N. Tiwari, T. Schnabel, E. Ahlswede. Solar Energy Materials and Solar Cells 119 (2013) 181-189.

[12] Todorov, T., & Mitzi, D. B. (2010). Direct liquid coating of chalcopyrite light-absorbing layers for photovoltaic devices. European Journal of Inorganic Chemistry, 2010(1), 17-28.

[13] Roy, B., & Bandyopadhyay, S. (2018). The design strategies and mechanisms of fluorogenic and chromogenic probes for the detection of hydrazine. Analytical Methods, 10(10), 1117-1139.

[14] Sackheim, R. L., & Masse, R. K. (2014). Green propulsion advancement: challenging the maturity of monopropellant hydrazine. Journal of Propulsion and Power, 30(2), 265-276.

[15] Qijie Guo, Grayson M. Ford, Wei-Chang Yang, Bryce C. Walker, Eric A. Stach, Hugh W. Hillhouse, and Rakesh Agrawal. J. Am. Chem. Soc. 132 (2010) 17384–17386.

[16] Teodor Todorov, Oki Gunawan, S. Jay Chey, Thomas Goislard de Monsabert, Aparna Prabhakar, David B. Mitzi. Thin Solid Films 519 (2011) 7378-7381.

[17] Roe, F. J. C., Grant, G. A., & Millican, D. M. (1967). Carcinogenicity of hydrazine and 1, 1-dimethylhydrazine for mouse lung. Nature, 216(5113), 375-376.

[18] Kush, P., & Deka, S. (2014). Photoelectrical properties of surfactant-free kesterite Cu 2 ZnSnSe 4 hydrophilic nanocrystal ink and the stability in polar solvents. Journal of nanoparticle research, 16(9), 2600.

[19] Ritchie, C., Chesman, A. S. R., Jasieniak, J., & Mulvaney, P. (2019). Aqueous synthesis of Cu2ZnSnSe4 nanocrystals. Chemistry of Materials, 31(6), 2138-2150.

[20] Valls, R. M., Lyubenova, T. S., Roures, I. C., Oliveira, L., Chiva, D. F., & Castelló, J. B. C. (2017). Easy and low-cost aqueous precipitation method to obtain Cu2ZnSn (S, Se) 4 thin layers. Solar Energy Materials and Solar Cells, 161, 432-438.

[21] Tan, L., Zhang, Y., Chen, Y., & Chen, Y. (2015). Homogeneous Cu2ZnSnSe4 nanocrystals/graphene oxide nanocomposites as hole transport layer for polymer solar cells. Chemical Physics Letters, 622, 1-8.

[22] Wang, J. J., Hu, J. S., Guo, Y. G., & Wan, L. J. (2012). Wurtzite Cu 2 ZnSnSe 4 nanocrystals for high-performance organic–inorganic hybrid photodetectors. NPG Asia Materials, 4(1), e2-e2.

[23] Shibayama, N., Zhang, Y., Satake, T., & Sugiyama, M. (2017). Modelling of an equivalent circuit for Cu 2 ZnSnS 4-and Cu 2 ZnSnSe 4-based thin film solar cells. RSC Advances, 7(41), 25347-25352.

[24] Sampath, S., Uchida, H., & Yoneyama, H. (1994). Photocatalytic degradation of gaseous pyridine over zeolite-supported titanium dioxide. Journal of Catalysis, 149(1), 189-194.

[25] Berglund, B., Höglund, A., & Esfandabad, H. S. (2012). A bisensory method for odor and irritation detection of formaldehyde and pyridine. Chemosensory Perception, 5(2), 146-157.

[26] Ito, N., Hasegawa, R., Imaida, K., Tamano, S., Hagiwara, A., Hirose, M., & Shirai, T. (1997). Carcinogenicity of 2-amino-1-methyl-6-phenylimidazo [4, 5-b] pyridine (PhIP) in the rat. Mutation Research/Fundamental and Molecular Mechanisms of Mutagenesis, 376(1-2), 107-114.

[27] Shahiduzzaman, M., Hossain, M. I., Visal, S., Kaneko, T., Qarony, W., Umezu, S., ... & Isomura, M. (2021). Spray Pyrolyzed TiO 2 Embedded Multi-Layer Front Contact Design for High-Efficiency Perovskite Solar Cells. *Nano-Micro Letters*, *13*(1), 1-17.

[28] Hossain, M. I., Saleque, A. M., Ahmed, S., Saidjafarzoda, I., Shahiduzzaman, M., Qarony, W., ... & Tsang, Y. H. (2021). Perovskite/perovskite planar tandem solar cells: A comprehensive guideline for reaching energy conversion efficiency beyond 30%. *Nano Energy*, *79*, 105400.

[29] Cho, A., Song, H., Gwak, J., Eo, Y. J., Yun, J. H., Yoon, K., & Ahn, S. (2014). A chelating effect in hybrid inks for non-vacuum-processed CuInSe 2 thin films. Journal of Materials Chemistry A, 2(14), 5087-5094.

[30] Dimitrievska, M., Fairbrother, A., Saucedo, E., Pérez-Rodríguez, A., & Izquierdo-Roca, V. (2016). Secondary phase and Cu substitutional defect dynamics in kesterite solar cells: impact on optoelectronic properties. Solar Energy Materials and Solar Cells, 149, 304-309.

[31] Olgar, M. A., Atasoy, Y. A. V. U. Z., Başol, B. M., Tomakin, M., Aygun, G., Ozyuzer, L., & Bacaksız, E. (2016). Influence of copper composition and reaction temperature on the properties of CZTSe thin films. Journal of Alloys and Compounds, 682, 610-617.

[32] Just, J., Sutter-Fella, C. M., Lützenkirchen-Hecht, D., Frahm, R., Schorr, S., & Unold, T. (2016). Secondary phases and their influence on the composition of the kesterite phase in CZTS and CZTSe thin films. Physical Chemistry Chemical Physics, 18(23), 15988-15994.

[33] Wibowo, R. A., Yoo, H., Hölzing, A., Lechner, R., Jost, S., Palm, J., ... & Hock, R. (2013). A study of kesterite Cu2ZnSn (Se, S) 4 formation from sputtered Cu–Zn–Sn metal precursors by rapid thermal processing sulfo-selenization of the metal thin films. Thin Solid Films, 535, 57-61.

[34] Kumar, V., Dutta, A., & Singh, U. P. (2020). Optimization of selenization parameters for fabrication of CZTSe thin film. Superlattices and Microstructures, 106578.

[35] K. Sobayel, Md. Akhtaruzzaman, et. al. (2019). A comprehensive defect study of tungsten disulfide (WS2) as electron transport layer in perovskite solar cells by numerical simulation. Results in Physics, Volume 12, Pages 1097-1103.

[36] K. Sobayel, N. Amin, et. al. (2020). Efficiency enhancement of CIGS solar cell by WS2 as window layer through numerical modelling tool. Solar Energy, Volume 207, 2020.

[37] K. Sobayel et. al. (2018). Numerical modelling on prospective buffer layers for tungsten di-sulfide (WS2) solar cells by scaps-1d. Chalcogenide Letters, Vol. 15, No. 6, p. 307 – 315.

[38] Yakushev, M. V., Sulimov, M. A., Márquez-Prieto, J., Forbes, I., Krustok, J., Edwards, P. R. & Martin, R. W. (2017). Influence of the copper content on the optical properties of CZTSe thin films. Solar Energy Materials and Solar Cells, 168, 69-77.

[39] G. Kartopu, B.L. Williams, V. Zardetto, A.K. Gürlek, A.J. Clayton, S. Jones, W.M.M. Kessels, M. Creatore, S.J.C. Irvine, Enhancement of the photocurrent and efficiency of CdTe solar cells suppressing the front contact reflection using a highly-resistive ZnO buffer layer, Solar Energy Materials and Solar Cells, Volume 191, 2019, Pages 78-82.

[40] F.T. Munna, Vidhya Selvanathan, K. Sobayel, et al., Diluted chemical bath deposition of CdZnS as prospective buffer layer in CIGS solar cell, Ceramics International, 2020.

[41] Khattak, Y.H., Baig, F., Toura, H. *et al.* CZTSe Kesterite as an Alternative Hole Transport Layer for $MASnI_3$ Perovskite Solar Cells. *Journal of Elec Material* **48,** 5723–5733 (2019).

[40] Wang, Wei; Winkler, Mark T.; Gunawan, Oki; Gokmen, Tayfun; Todorov, Teodor K.; Zhu, Yu; Mitzi, David B. (2014). Device Characteristics of CZTSSe Thin-Film Solar Cells with 12.6% Efficiency. Advanced Energy Materials, 4(7), n/a–n/a. doi:10.1002/aenm.201301465.

[41] Li, Xinchen; Zhuang, Daming; Zhang, Ning; Zhao, Ming; Yu, Xinping; Liu, Peng; Wei, Yaowei; Ren, Guoan (2019). Achieving 11.95% efficient CuZnSnSe solar cells fabricated by sputtering Cu-Zn-Sn-Se quaternary compound target with selenization process. Journal of Materials Chemistry A. doi:10.1039/C9TA00385A

[42] Hossain, M. I., Hasan, A. M., Qarony, W., Shahiduzzaman, M., Islam, M. A., Ishikawa, Y., ... & Tsang, Y. H. (2020). Electrical and Optical Properties of Nickel-Oxide Films for Efficient Perovskite Solar Cells. *Small Methods*, *4*(9), 2000454.

[43] Hossain, M. I., Qarony, W., Jovanov, V., Tsang, Y. H., & Knipp, D. (2018). Nanophotonic design of perovskite/silicon tandem solar cells. *Journal of Materials Chemistry A*, *6*(8), 3625-3633.

[44] Liyong Yao, Jianping Ao, Ming-Jer Jeng, Jinlian Bi, Shoushuai Gao, Guozhong Sun, Qing He, Zhiqiang Zhou, Yun Sun, Liann-Be Chang, A CZTSe solar cell with 8.2% power conversion efficiency fabricated using electrodeposited Cu/Sn/Zn precursor and a three-step selenization process at low Se pressure, Solar Energy Materials and Solar Cells, Volume 159, 2017.